Computation of Three-Dimensional Turbulent Shear Flows in Corners

J. J. Gorski,* T. R. Govindan,† and B. Lakshminarayana‡
The Pennsylvania State University, University Park, Pennsylvania

A numerical technique developed for the solution of the steady Navier-Stokes equations using a "space marching" algorithm has been used to predict a complex, three-dimensional turbulent flow. The scheme has been designed to calculate flows with a dominant flow direction, in three-dimensional geometries, and has been used successfully to predict laminar flows. This paper is concerned with the extension of this technique to calculate turbulent flows in the corner region of the wingbody junction using both the algebraic eddy viscosity and the k-ϵ turbulence models. The effects of different boundary conditions for the streamwise velocity at a solid boundary, used in many turbulent flow computations, are also considered. In the flow cases computed in this paper using a law of the wall boundary condition at solid boundaries, the k-ϵ model showed no distinct advantages over the simpler algebraic viscosity model. However, the k-ϵ model provided much better results for the cases computed with the more realistic no-slip boundary condition.

Nomenclature

$E,F,G,$ Q,R,T	= flux vectors in the Navier-Stokes equations, Eq. (1)
e_i	= specific internal energy normalized by $\rho_\infty U_\infty^2$
J	= Jacobian of the coordinate transformation
k	= turbulent kinetic energy normalized by U_∞^2
L	= characteristic length of the body or flow
P	= production of turbulent kinetic energy
p	= static pressure
q	= dependent flux vector, Eq. (1)
R_e	= Reynolds number based on ρ_∞, U_∞, L, and μ
u,v,w	= velocity components in x,y,z directions, respectively, normalized by U_∞
U	= velocity in the principal (x) direction normalized by U_∞
U_R	= resultant velocity normalized by U_∞
u_τ	= friction velocity ($\sqrt{\tau_w/\rho}$) normalized by U_∞
x,y,z	= Cartesian coordinates normalized by L
X,Y,Z	= physical distances, cm
y_l	= distance to the nearest wall normalized by L
γ	= specific heat ratio
ϵ	= dissipation rate normalized by U_∞^3/L
κ	= von Kármán constant
μ	= molecular viscosity normalized by μ_∞
μ_t	= eddy viscosity normalized by μ_∞
ξ,η,ζ	= body-fitted coordinate system
$\xi_x,\xi_y,\eta_x,$ η_y,ζ_z	= metrics of the coordinate transformation, Eq. (2)
ρ	= density normalized by ρ_∞
τ	= shear stress normalized by $\rho_\infty U_\infty^2$
ω	= vorticity

Subscripts

w	= wall
∞	= freestream value
max	= maximum value

Presented as Paper 83-1733 at the AIAA 16th Fluid and Plasma Dynamics Conference, Danvers, Mass. July 12-14, 1983; revision received June 20, 1984.

*NASA CFD Trainee, Department of Aerospace Engineering.

†Graduate Assistant, Department of Aerospace Engineering. Member AIAA.

‡Director of Computational Fluid Dynamics Studies and Professor of Aerospace Engineering, Department of Aerospace Engineering. Fellow AIAA.

Introduction

COMPLEX flows of the type found in curved ducts and corners are markedly influenced by three-dimensionality, pressure gradients, and viscous and turbulence effects. Curvature and pressure gradients induce strong secondary flows of the first kind. The computation of such flows requires algorithms that incorporate all the mean flow effects and a turbulence closure that can model the complexities of the flow turbulence.

The gradients of flow variables in both transverse directions, for the flows described above, are important and cannot be neglected. Hence, the conventional three-dimensional boundary-layer-type solution schemes cannot be adopted for such flows. Time-marching solutions to the Navier-Stokes equations are too prohibitive for three-dimensional geometries.

The parabolic marching methods have been successfully employed to predict flows with a dominant flow direction.[1] Extensions of these techniques to compute flow with a strong pressure gradient require an additional equation for pressure, which is solved by iteration.[2] The problem of properly satisfying the local continuity in the entire flowfield through the iterations remains in partially parabolic methods. A further drawback in the parabolic method is the separation of the governing equations into individual equations during the solution and the use of an iterative scheme to couple the equations.

The numerical scheme used in this paper, which was developed by Govindan,[3] utilizes the strengths of previous methods and overcomes their weaknesses. The Navier-Stokes equations have been posed as an initial value problem in the streamwise direction by neglecting the effects of streamwise diffusion and by treating the streamwise pressure gradient as a known source term. The fully coupled system of equations has been solved by a noniterative algorithm at each streamwise step of the computation, thus "space marching" the solution. This provides a fully coupled system of equations in the transverse plane and can be solved by fully implicit schemes. This technique has been used in the present computations.

An important element of calculating flows described above is turbulence modeling. The simplest models used for the calculation of turbulent shear flows are algebraic eddy viscosity models, referred to as eddy viscosity models in the rest of this paper. These models have been developed primarily for calculating two-dimensional flows. However, they contain a large amount of empiricism that is not generally valid in complex three-dimensional flows. Three other types of turbulence models have been developed in the literature that are applicable to this class of problems: two-equations models, algebraic Reynolds stress models, and the full Reynolds stress transport equations. The full Reynolds stress transport equations involve the solution of six additional partial differential equations for the stresses and greatly increase an already formidable amount of numerical computation. The algebraic Reynolds stress models have been developed as an attractive alternative to the full Reynolds stress equations. However, these models have not been refined sufficiently to make them generally applicable to three-dimensional flowfields. In particular, more work needs to be done before these models can adequately calculate near-wall turbulence.[4] Consequently, this paper will examine the use of algebraic eddy viscosity and two-equation k-ϵ turbulence models in three-dimensional shear flow computations.

Another element is the choice of an appropriate test case. At the Stanford Workshop[5] only three three-dimensional cases were accepted: 1) a duct with a 90 deg bend, which was not well predicted by any of the computers; 2) a straight duct with secondary flow of the second kind, which cannot be predicted using k-ϵ or eddy viscosity models; and 3) flow past a wingbody junction. Because of the restrictions on the turbulence models and the difficulty of the 90 deg bend, the wingbody junction of Shabaka[6] was chosen at the best test case for the calculations. As suggested at the Stanford Workshop,[5] the calculations were started downstream of the wing leading edge using experimental data as the initial conditions. This poses an immediate problem as there was no data very near the wall. Consequently, most of the initial conditions within the boundary layer are interpolated values.

As already stated, this paper will investigate how well an eddy viscosity model and a k-ϵ model perform in prediciting the wingbody junction flow of Shabaka.[6] This paper will also compare two different boundary conditions at a wall: the no-slip boundary condition and a law of the wall boundary condition. Finally, this paper will investigate the importance of how close the first grid point must be to the wall.

The Governing Equations and the Numerical Scheme

The governing equations and the numerical technique have been developed in Ref. 3 and only a brief summary will be given here. The Navier-Stokes equations for compressible flow in a rectangular coordinate system (x,y,z) can be written in nondimensional form as

$$\frac{\partial E(q)}{\partial x}+\frac{\partial F(q)}{\partial y}+\frac{\partial G(q)}{\partial z} = \frac{1}{Re}\left[\frac{\partial Q(q)}{\partial x}+\frac{\partial R(q)}{\partial y}+\frac{\partial T(q)}{\partial z}\right] \tag{1}$$

The vectors E, F, and G contain the convective terms and Q, R, and T contain the viscous diffusion terms. The dependent vector q is chosen as

$$q=[\rho,\rho u,\rho v,\rho w,\rho e_i]^T$$

where u, v, and w are the velocities in the x, y, and z directions, respectively, normalized by the freestream velocity U_∞. The fluxing of internal energy ρe_i was used as the dependent variable instead of the more commonly used total energy e. The use of ρe_i instead of e as an independent variable was found to improve the solution for low Mach number flows, since the pressure is directly proportional to the internal energy.

Equation (1) is transformed to a body-fitted coordinate system and the flow domain mapped to a cube in which the computations are carried out. Thus, transformation can be described as

$$\xi=\xi(x,y), \qquad \eta=\eta(x,y), \qquad \zeta=\zeta(z) \tag{2}$$

where ξ is the coordinate in a near streamwise direction and η and ζ the coordinates in the transverse plane that is approximately normal to the streamwise direction. The viscous diffusion terms in the ξ direction can be dropped in comparison to the diffusion terms in the transverse directions, an approximation valid in high Reynolds number flows with a dominant flow direction. The transformed equations can be kept in a form similar to Eq. (1),

$$\frac{\partial \hat{E}}{\partial \xi}+\frac{\partial \hat{F}}{\partial \eta}+\frac{\partial \hat{G}}{\partial \zeta}=\frac{1}{Re}\left[\frac{\partial \hat{R}}{\partial \eta}+\frac{\partial \hat{T}}{\partial \zeta}\right] \tag{3}$$

where

$$J\hat{E}=(\xi_x E+\xi_y F), \quad J\hat{F}=(\eta_x E+\eta_y F), \quad J\hat{G}=(\zeta_z G),$$
$$J\hat{R}=(\eta_x Q+\eta_y R), \quad J\hat{T}=(\zeta_x T)$$

and J is the Jacobian of the coordinate transformation. An example of the above flux vectors, the streamwise flux vector, is given by

$$\hat{E}=\frac{1}{J}\left|\begin{matrix}\rho U\\ \rho u U+\xi_x p\\ \rho v V+\xi_y p\\ \rho w U\\ (e+p)U\end{matrix}\right|$$

where U is the contravariant velocity,

$$U=\xi_x u+\xi_y v$$

and e is the total energy

$$e=\rho[e_i+0.5(u^2+v^2+W^2)]$$

Details of the above equations and the transformations can be found in Refs. 3 and 8. The equation of state is needed to close the system of Eq. (3) and is given by

$$p=(\gamma-1)\rho e_i$$

Equation (3) is a well-posed initial value problem in ξ if the eigenvalues of the Jacobian matrix of $\hat{E}$, $\partial\hat{E}/\partial q$, are all positive.[3,7] As shown by Schiff and Steger,[8] one eigenvalue of the Jacobian matrix of $\hat{E}$ is negative for subsonic cases, leading to an exponentially growing solution—an ill-posed initial value problem. The eigenvalues can all be made positive by removing the pressure dependency from the Jacobian matrix of $\hat{E}$. The eigenvalues are now positive, provided the streamwise velocity is positive, restricting the method to unseparated flow. The pressure terms are separated from vector $\hat{E}$ to form a known source vector $\hat{E}_p$ dependent on assumed pressure p_s. The first term in Eq. (3) is written as

$$\frac{\partial \hat{E}(q)}{\partial \xi}=\frac{\partial \hat{E}_s(q)}{\partial \xi}+\hat{E}_p(p_s)$$

where $\hat{E}_p(p_s)$ is the known source vector and $\hat{E}_p$ the unknown vector having all its eigenvalues coincident and equal to the contravariant velocity.

Removing the dependency of the Jacobian matrix of $\hat{E}$ requires that the streamwise pressure gradient be treated as a known source term in the equations. However, only the streamwise pressure gradient need be treated as known in the equations. The transverse pressure gradients can be treated implicitly with the transverse velocities and can be computed from the equations. This is an important requirement for computing flows with strong secondary velocities.

A marching scheme in the ξ direction can now be formulated for Eq. (3) when posed as an initial value problem as described above. The linearized block implicit method of Briley and McDonald[9] has been adopted for this purpose. Details of the algorithm can be found in Refs. 3 and 9.

A computer code for the above method has been written and is described in Ref. 3. The code and the method have been developed primarily to predict internal flows of the kind found in curved ducts and turbomachinery rotor passages, but is general enough to handle many external flow cases as well. The method has been tested against different internal and external laminar flow cases. Details of the method, the computer code, and the test cases can be found in Ref. 3. It must be emphasized that the method, as described here, requires the specification of the streamwise pressure gradient in the entire flowfield.

The effects of turbulence are simulated by introducing an eddy viscosity μ_t. The molecular viscosity is replaced by the effective viscosity $(\mu+\mu_t)$ in the Navier-Stokes equation (3). In the present paper, two different methods were used for calculating the eddy viscosity, a simple algebraic eddy viscosity model and a two-equation k-ϵ model described below.

Turbulence Closure Models

Eddy Viscosity Model

The algebraic eddy viscosity model used is that developed by Baldwin and Lomax.[10] It is a two-layer eddy viscosity model in which an eddy viscosity is calculated for an inner and an outer region. The inner region is based on the Prandtl-Van Driest formulation

$$(\mu_t)_{\text{inner}} = \rho \ell^2 |\omega| Re \tag{4}$$

where

$$\ell = \kappa y_l [1-\exp(-y^+/A^+)], \qquad y^+ = (\rho_w u_\tau y_l/\mu_w) R_e$$

and where $|\omega|$ is the magnitude of the vorticity given by

$$|\omega| = \sqrt{\left(\frac{\partial u}{\partial y}-\frac{\partial v}{\partial x}\right)^2 + \left(\frac{\partial v}{\partial z}-\frac{\partial w}{\partial y}\right)^2 + \left(\frac{\partial w}{\partial x}-\frac{\partial u}{\partial z}\right)^2}$$

The eddy viscosity for the outer region is given by

$$(\mu_t)_{\text{outer}} = K C_{cp} F_{\text{wake}} F_{\text{KLEB}}(y_l) R_e \tag{5}$$

where $F_{\text{wake}} = Y_{\max} F_{\max}$ or $C_{wk} Y_{\max} U_D^2 / F_{\max}$, the smaller of the two values.

$F_{\max}$ is the maximum value of the relation

$$F(y)_l = y_l |\omega| [1-\exp(-y^+/A^+)]$$

and $Y_{\max}$ is y_l at that point. Also

$$F_{\text{KLEB}}(y_l) = [1+5.5(C_{\text{KLEB}} y_l / y_{\max})^6]^{-1}$$

and

$$U_D = (\sqrt{u^2+v^2+w^2})_{\max}$$

It is necessary to specify the folowing constants: $A^+ = 26$, $C_{cp} = 1.6$, $C_{\text{KLEB}} = 0.3$, $C_{wk} = 0.25$, $\kappa = 0.4$, and $K = 0.0168$.

Rather than matching the inner and outer regions, the eddy viscosity was calculated at every point using both Eqs. (4) and (5). The smaller of the two eddy viscosities was then used in Eq. (3). Three-dimensional corner geometries were treated as two two-dimensional configurations and the eddy viscosity corresponding to each wall was calculated as described above. The eddy viscosities calculated from each wall were then compared and the smaller value was used in Eq. (3). This procedure would normally use the eddy viscosity calculated from the nearest wall.

The algebraic eddy viscosity models are simple to use and add little computation to the numerical scheme. This simplicity comes largely from the fact that they have been developed for two-dimensional flows over simple surfaces. This leads to the restriction that they are not generally applicable to three-dimensional flows. Consequently, it would be expected that the algebraic eddy viscosity model would be inadequate for three-dimensional flows, especially in corner regions. To overcome this problem, more complex models have been developed and continue to be developed. One model that has been used successfully to predict many flows is the two-equation k-ϵ model. Although more difficult and expensive to use, the k-ϵ model is, in general, more suitable for three-dimensional flows.

k-ϵ Model

The k-ϵ model used here was that described by Galmes and Lakshminarayana[11] and is based on the model developed by Jones and Launder.[12] To be consistent with the mean flow equations, the kinetic energy and dissipation equations have been transformed to a body-fitted coordinate system. These equations are also marched in space, making it necessary to neglect streamwise diffusion terms. The kinetic energy and dissipation equations can be written in a form similar to Eq. (3),

$$\frac{\partial A}{\partial \xi}+\frac{\partial B}{\partial \eta}+\frac{\partial C}{\partial \zeta}=\frac{1}{Re}\left[\frac{\partial M}{\partial \eta}+\frac{\partial N}{\partial \zeta}+S\right] \tag{6}$$

where

$$A=\frac{1}{J}\begin{bmatrix}\xi_x\rho k u+\xi_y \rho k v\\ \xi_x \rho\epsilon u+\xi_y\rho\epsilon v\end{bmatrix} \qquad B=\frac{1}{J}\begin{bmatrix}\eta_x\rho k u+\eta_y\rho k v\\ \eta_x\rho\epsilon u+\eta_y\rho\epsilon v\end{bmatrix}$$

$$C=\frac{1}{J}\begin{bmatrix}\zeta_z\rho k w\\ \zeta_z\rho\epsilon w\end{bmatrix} \qquad M=\frac{1}{J}\begin{bmatrix}\eta_y^2\mu_k\dfrac{\partial k}{\partial\eta}+\eta_x^2\mu_k\dfrac{\partial k}{\partial \eta}\\ \eta_y^2\mu_\epsilon\dfrac{\partial\epsilon}{\partial\eta}+\eta_x^2\mu_\epsilon\dfrac{\partial\epsilon}{\partial\eta}\end{bmatrix}$$

$$N=\frac{1}{J}\begin{bmatrix}\zeta_z^2\mu_k\dfrac{\partial k}{\partial\zeta}\\ \zeta_z^2\mu_\epsilon\dfrac{\partial\epsilon}{\partial\zeta}\end{bmatrix} \qquad S=\frac{1}{J}\begin{bmatrix}P-\rho\epsilon R_e\\ \dfrac{C_1\epsilon P}{k}-\dfrac{C_2 f_1\rho\epsilon^2}{k}R_e\end{bmatrix} \tag{7}$$

and where $\mu_k=(\mu+\mu_t/\sigma_k)$; $\mu_\epsilon=\mu+\mu_t/\sigma_\epsilon$. P represents the production of kinetic energy and a simplified form of it is used as suggested by Arnal and Cousteix[13] and Rodi et al.,[14]

$$\frac{P}{J}=\rho\mu_t\left(\frac{\partial}{\partial\eta}\frac{\eta_y u}{J}\right)+\rho\mu_t\left(\frac{\partial}{\partial\zeta}\frac{\zeta_z u}{J}\right)^2 \tag{8}$$

The k-ϵ model still employs the eddy viscosity/diffusivity concept as it relates eddy viscosity to the kinetic energy and

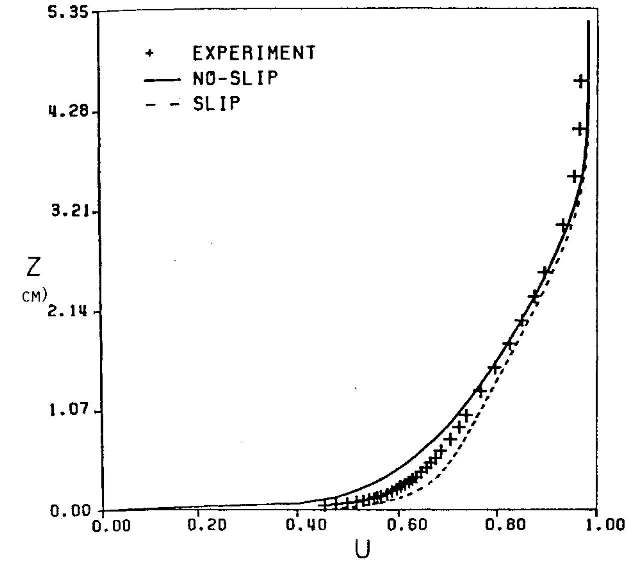

Fig. 1 Comparison of streamwise velocity using slip and no-slip boundary conditions for flat plate.

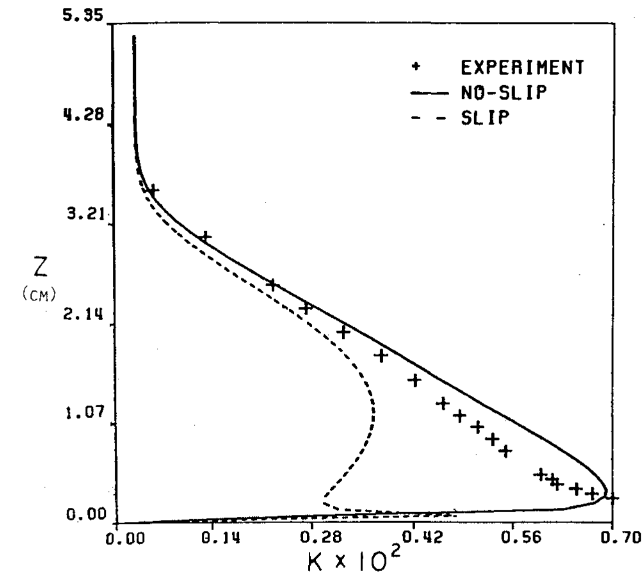

Fig. 2 Comparison of turbulent kinetic energy using slip and no-slip boundary conditions for flat plate.

dissipation by

$$\mu_t = C_\mu f_\mu \rho \frac{k^2}{\epsilon} R_e \tag{9}$$

To solve the above turbulence model, the following constants are specified: $\sigma_k = 1.0$, $\sigma_\epsilon = 1.3$, $C_1 = 1.44$, $C_2 = 1.92$, and $C_\mu = 0.09$. Wall vicinity effects are introduced by using the following functions prescribed by Jones and Launder[12]:

$$f_1 = 1.0 - \exp(-R_T^2)$$

$$f_\mu = \exp[-3.4/(1.0 + R_T/50)^2], \quad R_T = \rho k^2/\mu\epsilon$$

Although this constitutes a low Reynolds number form of the k-ϵ model, the calculation of kinetic energy and dissipation was not carried to the wall. A wall function was used to specify kinetic energy and dissipation at the first point away from the wall. This calculated kinetic energy and dissipation were then used as boundary conditions for Eq. (6). The wall

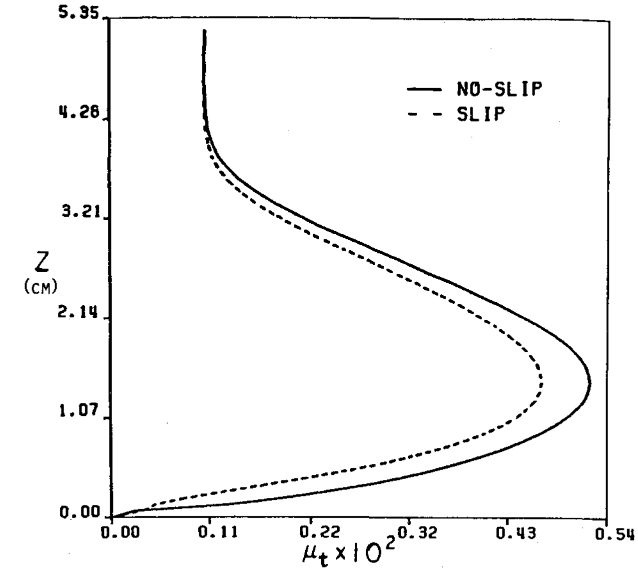

Fig. 3 Comparison of eddy viscosities calculated using slip and no-slip boundary conditions for flat plate.

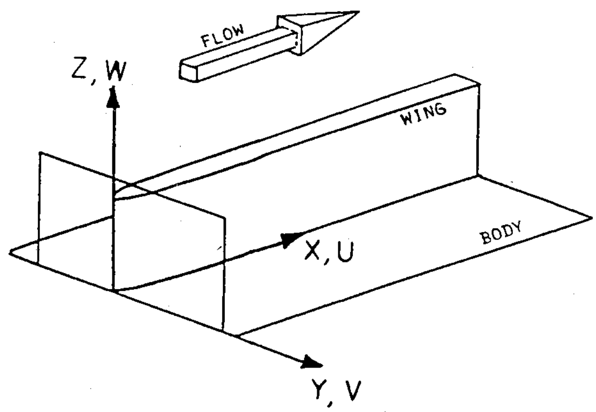

Fig. 4 Wingbody junction of Shabaka.[6]

function used[14] relates the resultant velocity parallel to the wall, the kinetic energy, and the dissipation rate to the resultant friction velocity by the following relations:

$$\frac{U_R}{u_\tau} = \frac{1}{\kappa} \ln\left(\frac{9u_\tau y_l}{\mu} R_e\right), \quad \kappa = \frac{u_\tau^2}{\sqrt{C_\mu}}, \quad \epsilon = \frac{u_\tau^3}{\kappa y_l} \tag{10}$$

The above equations were solved using the same method used for the Navier-Stokes equations. Rather than solving the coupled equations, each equation was solved individually.

Boundary Conditions

As stated previously, it is necessary to specify the streamwise pressure gradient everywhere in the flowfield. At boundaries other than the walls, through flow conditions are used. At the walls, the transverse velocities are set to zero. Two different boundary conditions were used at the walls for the streamwise velocity. A true no-slip condition was applied by setting the streamwise velocity to zero on the wall. It is important to note that when the no-slip boundary condition was used, the wall functions were not used at the boundary except for defining the turbulent kinetic energy and the dissipation at the first point away from the wall. In particular, the streamwise velocity was not set at the first point away from the wall, but was computed from the governing equations. The second approach used a law of the wall to define a "slip" velocity at the wall, as suggested by Kreskov-

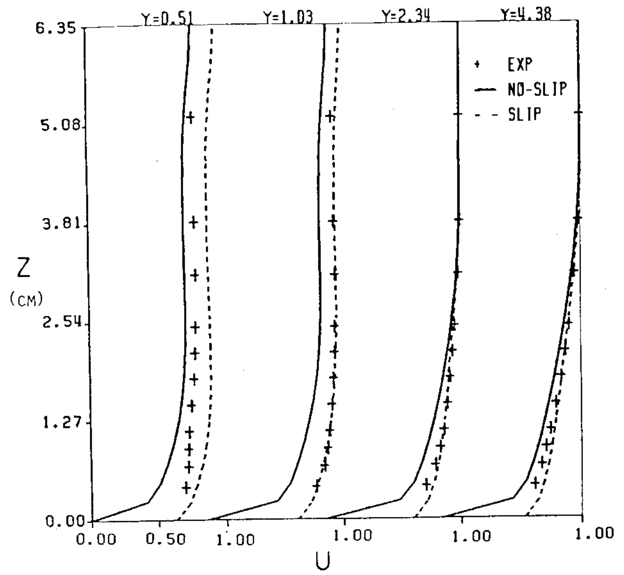

Fig. 5 Comparison of streamwise velocity using slip and no-slip boundary conditions at $x = 0.647$ m.

sky et al.[15] This was done using the relation

$$\frac{\partial U}{\partial y} = \frac{u_\tau}{\kappa y} \tag{11}$$

obtained from Eq. (10). This forces the velocities near the wall to follow the prescribed velocity on the wall given by Eq. (10). The transverse velocity components were still set to zero on the wall. Using this approach, the governing equations (3) are satisfied at the first point away from the wall. This approach seems equivalent to other methods that employ a wall function to specify the velocity at the first point away from the wall and is applied in this manner only for convenience. The law of the wall boundary condition is referred to as "slip" in all figures.

To test the computer code and validity of the turbulence models, a two-dimensional flow was calculated first. This served as a basis for comparison before solving the flowfield over the three-dimensional configuration.

Comparison between Predictions and Experimental Data

Flat Plate with Adverse Pressure Gradient

The first case considered here to validate the code and to check the turbulence model is the two-dimensional flow over a flat plate with an increasingly adverse pressure gradient measured by Samuel and Joubert.[16] This flow was used by workers at the Stanford Conference[5] to study the behavior of different turbulence models as the flow approached separation. As the separated flow is not of primary interest here, the experimental data at 1.44 m (from the leading edge of the flat plate) was used as initial conditions and the solution was computed up to 1.76 m downstream of the leading edge.

Figure 1 shows a comparison of the streamwise velocity using both of the previously mentioned boundary conditions with the k-ϵ model. The predictions are good. Discrepancies near the wall are about 2-3% of the streamwise velocity and slightly higher away from the wall in the inner regions of the boundary layer. The turbulent kinetic energy profiles computed with the two boundary conditions are shown in Fig. 2. The calculation using the no-slip boundary condition computes the kinetic energy very well, being only slightly higher in the inner regions of the boundary layer. The kinetic energy computed using the law of the wall significantly underpredicts the experimental values.

The eddy viscosity μ_t computed using the k-ϵ model, for both the law of the wall and no-slip boundary conditions, is shown in Fig. 3. This explains how two widely different kinetic energy profiles can predict nearly the same streamwise velocities. For the law of the wall case, the computed dissipation must be compensating for the poor kinetic energy to provide nearly the same eddy viscosity values for both types of boundary conditions.

Computations using the algebraic eddy viscosity model were also made and compared with the k-ϵ model. The eddy viscosity model produced nearly identical results to those obtained using the k-ϵ model. This would be expected as the eddy viscosity model was primarily developed for two-dimensional flow.

All previous calculations had been done with the first grid point near the edge of the viscous sublayer. A calculation was also made using the k-ϵ model, where the first grid point was a considerable distance from the viscous sublayer, but still within the law of the wall region. For the no-slip boundary condition, the streamwise velocity was significantly underpredicted, showing the importance of grid refinement. However, when the law of the wall boundary condition was used, there was not a significant amount of difference between the coarse and fine grids.

Summarizing, the two-dimensional calculations have shown that both turbulence models and boundary conditions work well. However, there is concern about the poor kinetic energy predicted using the law of the wall boundary condition, even though the calculated dissipation compensated for it. Finally, grid refinement has a much greater effect on the no-slip boundary condition than on the law of the wall boundary condition. Now that the performance and characteristics of the turbulence models and boundary conditions have been shown, we can proceed to the three-dimensional investigation.

Flow in the Region of a Wingbody Junction

The three-dimensional test case was the flow in the region of a wingbody junction measured by Shabaka.[6] The wing has a semielliptical leading edge followed by a section of constant thickness (Fig. 4). The boundary layer approaching the leading edge separates and forms a leading-edge horseshoe vortex that is then convected downstream along either side of the wing. To avoid the complexities of the flow at the leading edge, the calculations were started 0.187 m downstream of it using experimental data as the initial conditions, as suggested at the Stanford Conference.[5] This poses a problem as experimental measurements were not taken very near the wall, making it necessary to interpolate for a large portion of the boundary-layer regions, an important part of the flow. Because of this and computer limitations, it was necessary to use fairly coarse grids. Therefore, the solutions cannot be assumed to be entirely grid independent.

Calculations were initially carried out on a 20×20 transverse grid. For this grid, the points nearest the wall were at approximately $y^+ = 100$. Although this is not optimal because of computer limitations and the previously mentioned problems with the initial data plane, it was necessary to do most of the numerical experimentation on this grid. Figure 5 shows a comparison of the streamwise velocities computed using both boundary conditions with the k-ϵ model. The no-slip boundary condition leads to underpredicted values, while the law of the wall gives very good predictions except near the wing. These streamwise velocity predictions have similar trends to the two-dimensional predictions reported previously. For this calculation, the law of the wall boundary condition gave better results than the no-slip boundary condition. This may be due to the fact that the boundary layer is insufficiently resolved.

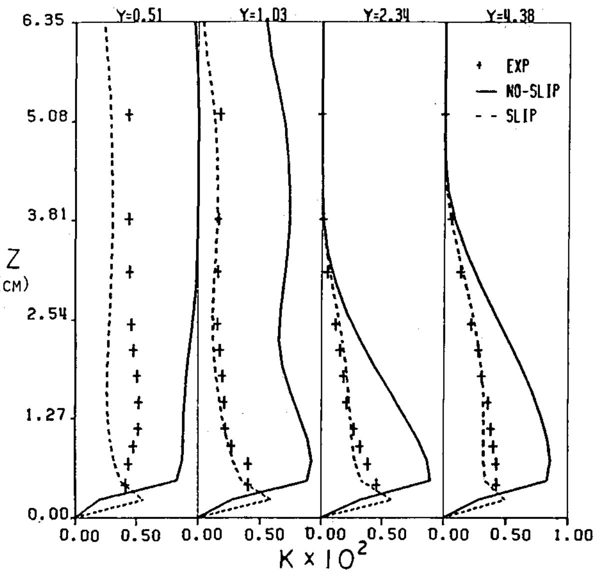

Fig. 6 Comparison of turbulence kinetic energy using the slip and no-slip boundary conditions at $x = 0.647$ m.

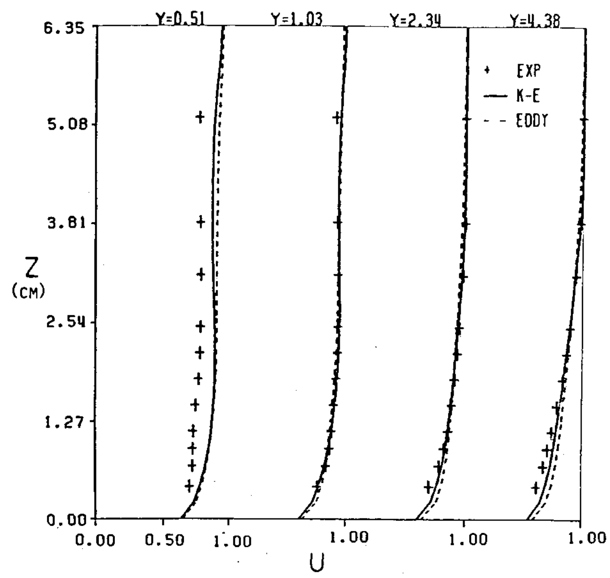

Fig. 8 Comparison of streamwise velocity computed using the k-ϵ and eddy viscosity turbulence models with slip boundary conditions at $x = 0.647$ m.

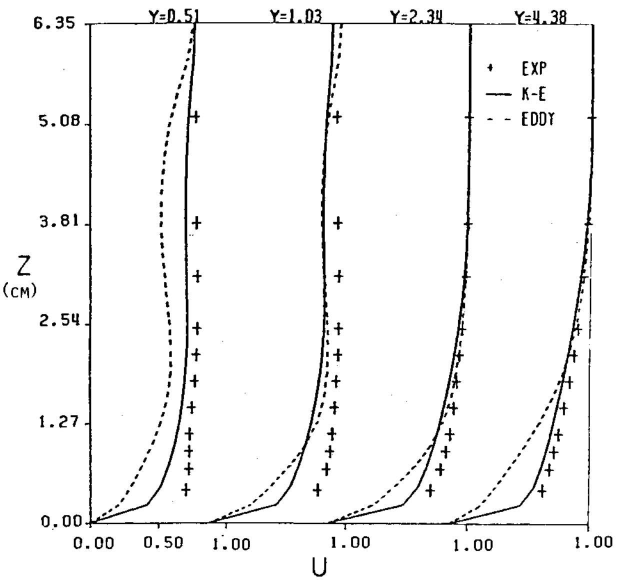

Fig. 7 Comparison of streamwise velocity computed using the k-ϵ and eddy viscosity turbulence models with no-slip boundary conditions at $x = 0.647$ m.

Figure 6 shows the comparison of kinetic energy for the two boundary conditions. Contrary to the two-dimensional calculations, the kinetic energy was predicted much better using the law of the wall rather than the no-slip boundary condition for this case. Some interesting observations can be made concerning the calculation of kinetic energy from these results. As stated previously, the kinetic energy is set at the first point away from the wall for all cases using the k-ϵ model. This value is then used as a boundary condition for the kinetic energy equation. In both test cases (two- and three-dimensional), the kinetic energy decreased from this value when the law of the wall boundary condition was used. Meanwhile, the kinetic energy increased, before decreasing, from this value when the no-slip boundary condition was used. This is a direct result of the boundary conditions on the streamwise velocity. The production of kinetic energy [Eq. (8)] is directly proportional to the streamwise velocity gradient normal to the wall. As can be seen from Figs. 1 and 5, this gradient is much lower for the law of the wall than the no-slip boundary condition. Hence, the production of kinetic energy is lower when using the law of the wall than when using the no-slip boundary condition. This is why the kinetic energy calculated using the law of the wall boundary condition is consistently lower than that calculated using the no-slip boundary condition. Because the production of kinetic energy is so small when using the law of the wall, it drops off immediately after the first preset value. Based on how poorly kinetic energy was predicted for the two-dimensional case when using the law of the wall, and on the above arguments, the authors think the good prediction of kinetic energy in the three-dimensional case is more by chance than anything else.

Figure 7 shows a comparison of streamwise velocities computed using the k-ϵ and eddy viscosity models with the no-slip boundary condition. The k-ϵ model performed significantly better. This is to be expected as the eddy viscosity model was developed primarily for two-dimensional flows.

Figures 8 and 9 exhibit some very startling results. Figure 8 is a comparison of streamwise velocities computed using the k-ϵ and eddy viscosity models with the law of the wall boundary condition. With this boundary condition the two turbulence models give nearly identical results. Even more startling is the fact that the eddy viscosities computed using both turbulence models (Fig. 9) are completely different. It is apparent that the application of the law of the wall boundary condition reduces the streamwise velocity gradient normal to the wall so much that the diffusion terms become negligible and the imposed velocity gradient is the dominant factor governing the boundary-layer development.

The results indicate that many of the computational problems encountered using a no-slip boundary condition would not be apparent when using a law of the wall boundary condition. This is why the simple algebraic model performed as well as the k-ϵ model when this boundary condition was used. This can lead to widespread use of turbulence models, and numerical codes themselves, that still have problems. However, for this case, the law of the wall boundary condition worked very well. For completeness, the calculation was carried down to $x = 1.254$ m. As can be seen from Fig. 10, the k-ϵ and law of the wall models still produce very good predictions of streamwise velocity. Many at the Stanford Conference[5] predicted the flowfield at this station using the parabolic marching method of Ref. 1 or modified versions of

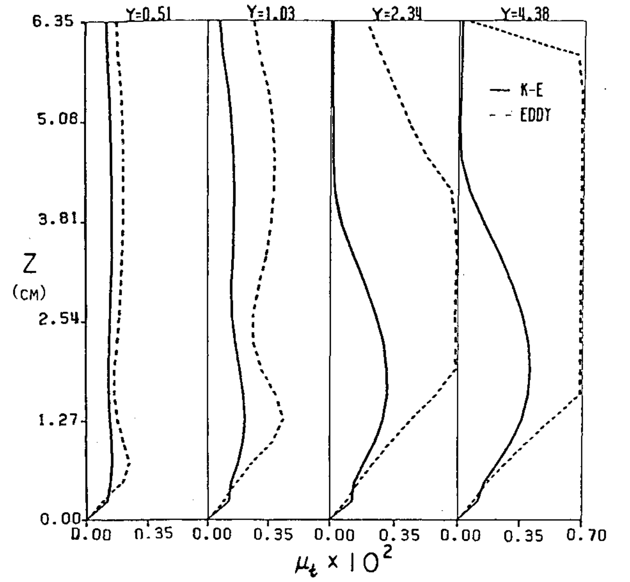

Fig. 9 Comparison of eddy viscosity computed using the two turbulence models at $x = 0.647$ m with slip boundary conditions.

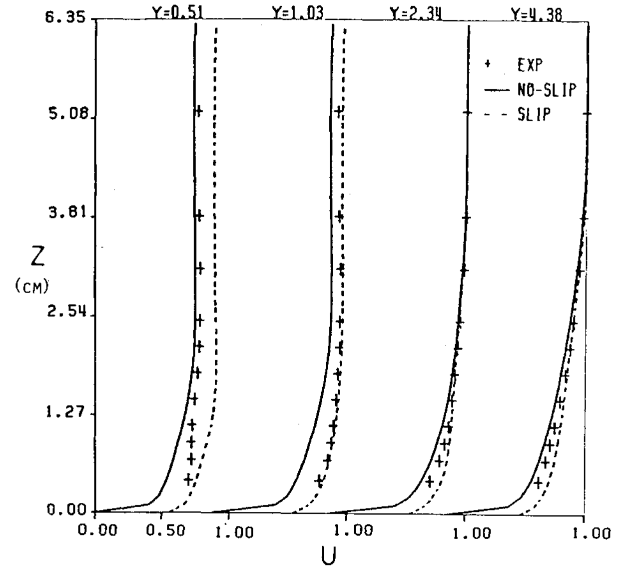

Fig. 11 Prediction of streamwise velocity computed using the k-ϵ model on a fine grid at $x = 0.647$ m.

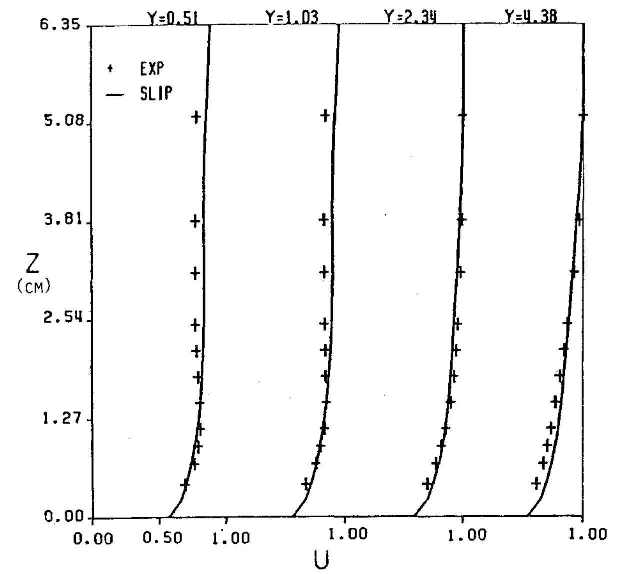

Fig. 10 Prediciton of streamwise velocity using the k-ϵ model and the slip boundary condition at $x = 1.254$ m.

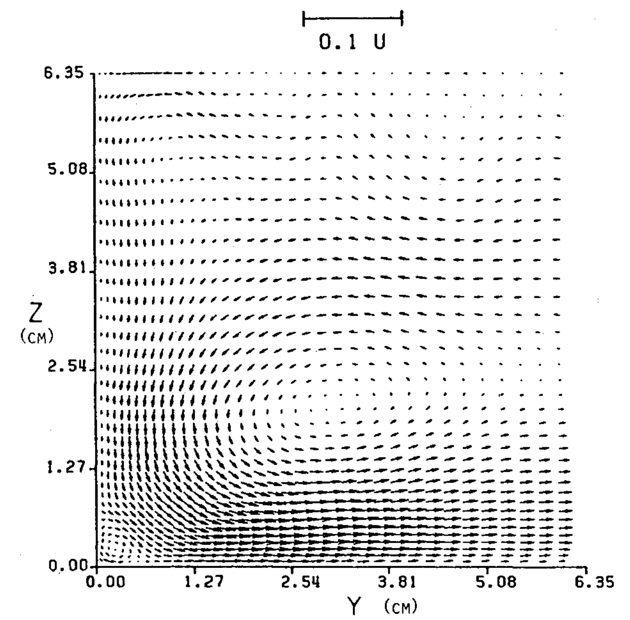

Fig. 12 Prediction of secondary velocities computed using the k-ϵ model on a fine grid with slip boundary conditions at $x = 0.647$ m.

it. The prediction of streamwise velocity was good, except in the regions close to the wing. The present predictions are better than those reported in Ref. 5, especially in the regions close to the wing. None of the earlier computations predicted the cross flows accurately.

Based on the previous arguments, the authors think a better test of the turbulence model and numerical code would be achieved by imposing the no-slip boundary condition. Therefore, the wingbody junction was also run on a 35×35 transverse grid. For this case, the first points away from the body are at about $y^+ = 30$ and from the wing about $y^+ = 50$. A finer grid than this would have been difficult to obtain because the wing boundary layer is so thin and also because of the necessity of interpolating for all points near the wingbody junction. Figure 11 shows the prediction of streamwise velocity using the k-ϵ model with both boundary conditions. As can be seen, there is very little difference between this solution and the previous coarse grid solution when the law of the wall boundary condition is used. This would indicate that when this boundary condition is used the placement of the first grid point away from the wall is not as crucial as commonly believed. However, there is a significant improvement over the coarse grid calculation when using the no-slip boundary condition. Now the solutions obtained with the no-slip boundary condition are as good as those obtained using the law of the wall. Figure 12 shows the secondary velocities computed using the k-ϵ model with the no-slip boundary condition. The choice of boundary conditions had little effect on the secondary velocities. The predicted secondary velocities are lower than the experimental velocities shown in Fig. 13. The predicted vortex in both cases has been pushed farther away from the wall than is indicated by the experimental results. This comparison of predictions with the experimental data must be viewed with some caution due to the interpolation required to define the secondary velocities on the initial plane of the computational grid. The sparse data in the corner could make the interpolation inaccurate. None of the previous investigators were able to

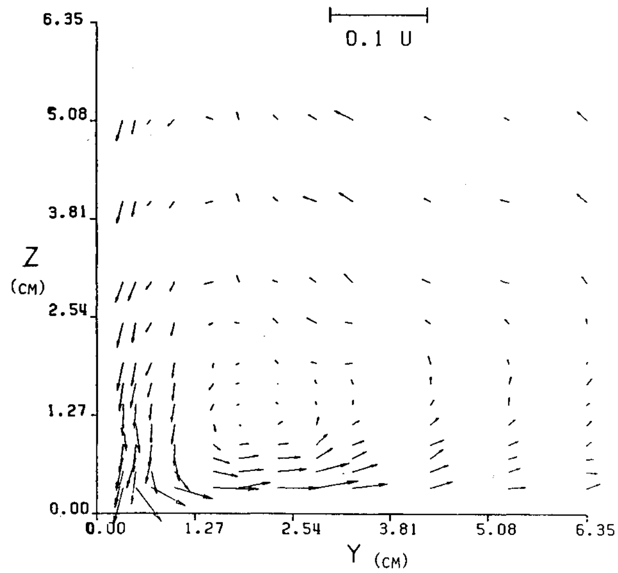

Fig. 13 Secondary velocities measured by Shabaka[6] at $x = 0.647$ m.

predict the transverse velocities accurately. It must be noted that the magnitudes of the maximum secondary velocities are less than 5% of the freestream velocity. The interpolated secondary velocities used as the initial condition are probably the reason for the small counter-rotating vortex generated in the corner. As would be expected, the fine grid provides a much better definition of the leading-edge vortex and the secondary velocities at the downstream station.

It is interesting to note that the formation of the corner eddy, secondary flow of the second kind, has been captured in the present numerical computation. None of the previous investigators reported these predictions.

Conclusions

1) The k-ϵ and the algebraic eddy viscosity models do equally well in predicting the two-dimensional flow over a flat plate subjected to an increasingly adverse pressure gradient.

2) In the case of the three-dimensional flow in a wingbody junction, the k-ϵ model does significantly better than the eddy viscosity model when a true no-slip boundary condition was used at solid boundaries. However, the eddy viscosity model does as well as the k-ϵ model when the law of the wall boundary conditions are prescribed at solid boundaries.

3) When using the law of the wall boundary conditions, varying the distance of the first point away from the wall had relatively little effect on the computations. Contrary to this, the distance had a significant effect on the computations when the no-slip boundary conditions was used.

4) Because of computer limitations, the law of the wall boundary conditions have seen widespread use in two- and three-dimensional calculations. This is justifiable as it has produced good results using relatively coarse grids, which could not be used when imposing the no-slip boundary condition. However, the imposed velocity gradient can have more of an effect on the solution than the turbulence models used. This can lead to problems when computing flows in which the two-dimensional law of the wall does not hold very well. (This probably accounts for poor predictions obtained for the 90 deg duct bend at the Stanford Conference.[5]) This can also lead to the false belief that a turbulence model works well even though it can have many hidden problems that would arise only if a no-slip boundary condition was used, as with the algebraic eddy viscosity in this case. Based on this, the authors think the law of the wall is a necessary boundary condition because of present computer limitations, but that care must be used when implementing this technique.

5) The wingbody junction is a complex flow with regions of negative eddy viscosity.[6] Because of this, a k-ϵ model should not work all that well. However, due to the fact that the boundary-layer growth was predicted so well and also that the definition of the vortex was reasonably well established while using the no-slip boundary condition with the fine grid, the authors think that the k-ϵ model and the code can be applied to complicated flowfields with good results. Based on this and the fact that distance from the wall did not matter when using the law of the wall, the authors' conclusions based on the coarse grid are realistic and question the validity of applying law of the wall boundary conditions indiscriminately.

Acknowledgments

J. Gorski was supported by the National Aeronautics and Space Administration through a Computational Fluid Dynamics Training Grant (NGT 39-009-802). The support for the computational work was provided by The Pennsylvania State University.

References

[1]Patankar, S. V. and Spalding, D. B., "A Calculation Procedure for Heat, Mass and Momentum Transfer in Three-Dimensional Parabolic Flows," *International Journal of Heat Transfer*, Vol. 15, 1972.

[2]Briley, W. R., "Numerical Methods for Predicting Three-Dimensional Flow Through Ducts," *Journal of Computational Physics*, Vol. 16, 1974.

[3]Govindan, T. R., "A Space-Marching Method for the Navier-Stokes Equations for Internal Flows," Ph.D. Thesis, Dept. of Aerospace Engineering, The Pennsylvania State University, University Park, Dec. 1983.

[4]Gorski, J. J., "Computation of the Turbulent Flow in the Corner of a Wingbody Junction," M.S. Thesis in Aerospace Engineering, The Pennsylvania State University, University Park, Dec. 1983.

[5]Kline, S. J. et al. (eds), *The 1980-81 AFOSR-HTTM Stanford Conference on Complex Turbulent Flows*, Stanford University, Stanford, Calif., 1982.

[6]Shabaka, I. M. M. A., "Turbulent Flow in a Simulated Wing-Body Junction," Ph.D. Thesis, Aeronautics Dept., Imperial College, London, 1979.

[7]Pulliam, J. H. and Steger, J. L., "On Implicit Finite-Difference Simulations of Three Dimensional Flow," *AIAA Journal*, Vol. 18, Feb. 1980, pp. 159-167.

[8]Schiff, L. B. and Steger, J. L., "Numerical Simulation of Steady Supersonic Viscous Flow," *AIAA Journal*, Vol. 18, Dec. 1980, pp. 1421-1430.

[9]Briley, W. R. and McDonald, H., "On the Structure and Use of Linearized Block Implicit and Related Systems," *Journal of Computational Physics*, Vol. 34, 1980, pp. 54-73.

[10]Baldwin, B. S. and Lomax, H., "Thin Layer Approximation and Algebraic Model for Separated Turbulent Flows," AIAA Paper 78-257, 1978.

[11]Galmes, J. M. and Lakshminarayana, B., "An Algebraic Reynolds Stress Model for Three-Dimensional Flows Over Curved Rotating Bodies," *AIAA Journal*, Oct. 1984.

[12]Jones, W. P. and Launder, B. E., "The Calculation of Low-Reynolds Number Phenomena with a Two-Equation Model of Turbulence," *Journal of Heat and Mass Transfer*, Vol. 16, 1973, pp. 1119-1130.

[13]Arnal, D. and Cousteix, J., "Numerical Study of Corner Flows," *Three Dimensional Turbulent Boundary Layers*, edited by H. H. Fernholz and E. Krause, Springer Verlag, New York, 1982, pp. 343-352.

[14]Rodi, W. et al., *The 1980-81 AFOSR-HTTM Stanford Conference on Complex Turbulent Flows*, Vols. I, II, and III, edited by S. J. Klein et al., Stanford University, Stanford, Calif., 1982.

[15]Kreskovsky, J. P., Briley, W. R., and McDonald, H., "Turbofan Forced Mixer-Nozzle Internal Flow Field," NASA CR 3494, 1982.

[16]Samuel, A. E. and Joubert, P. N., "A Boundary Layer Developing in an Increasingly Adverse Pressure Gradient," *Journal of Fluid Mechanics*, Vol. 66, 1975, p. 481.